Transmembrane Helix 5 Is Critical for the High Water Permeability of Aquaporin[†]

Michio Kuwahara,*[,‡] Itsuki Shinbo,[‡,§] Kazunori Sato,[‡] Yoshio Terada,[‡] Fumiaki Marumo,[‡] and Sei Sasaki[‡]

Second Department of Internal Medicine, School of Medicine, Tokyo Medical and Dental University, Tokyo 113-8519, and Laboratory for CAG Repeat Diseases, Brain Science Institute, RIKEN, Wako-shi, Saitama Prefecture 351-0198, Japan

Received July 21, 1999; Revised Manuscript Received September 23, 1999

ABSTRACT: Aquaporin-2 (AQP2), a vasopressin-regulated water channel, plays a major role in urinary concentration. AQP2 and the major intrinsic protein (MIP) of lens fiber are highly homologous (58% amino acid identity) and share a topology of six transmembrane helices connected by five loops (loops A−E). Despite the similarities of these proteins, however, the water channel activity of AQP2 is much higher than that of MIP. To determine the site responsible for this gain of activity in AQP2, several parts of MIP were replaced with the corresponding parts of AQP2. When expressed in *Xenopus* oocytes, the osmotic water permeability (P_f) of MIP and AQP2 was 48 and 245 × 10^{-4} cm/s, respectively. Substitutions in loops B−D failed to increase P_f, whereas substitution of loop E significantly increased P_f 1.5-fold. A similar increase in P_f was observed with the substitution of the front half of loop E. P_f measurements taken in a yeast vesicle expression system also confirmed that loop E had a complementary effect, whereas loops B−D did not. However, P_f values of the loop E chimeras were only ∼30% of that of AQP2. Simultaneous exchanges of loop E and a distal half of transmembrane helix 5 just proximal to loop E increased P_f to the level of that of AQP2. Replacement of helix 5 alone stimulated P_f 2.7-fold. Conversely, P_f was decreased by 73% when helix 5 of AQP2 was replaced with that of MIP. Moreover, P_f was stimulated 2.6- and 3.3-fold after helix 5 of AQP1 and AQP4 was spliced into MIP, respectively. Our findings suggested that the distal half of helix 5 is necessary for maximum water channel activity in AQP. We speculate that this portion contributes to the formation of the aqueous pore and the determination of the flux rate.

Water transport across the cell membrane is essential for the maintenance of the intracellular environment. Physiological evidence has shown that water molecules move through a selective pore. In fact, a water channel protein, now designated as aquaporin (AQP),[1] was first identified in 1992 (*1*). In intervening years, AQPs and their homologues, the major intrinsic protein (MIP) families, have been found repeatedly throughout nature (*2*). Ten AQPs (AQP0−9) are identified at present in mammals (*3*, *4*), and all of them have six transmembrane helices with three extracellular loops (A, C, and E) and two intracellular loops (B and D), as shown in Figure 1A (*5*, *6*). In the amino acid sequences of MIP and AQP, the first half is homologous to the second half and each repeat contains a conserved Asn-Pro-Ala (NPA) motif in cytoplasmic loop B and extracellular loop E (*7*). A number of investigators have examined the structure−function relationship in several AQPs. A site-directed mutagenesis study of AQP1 suggested that two NPA motifs of loops B and E participate in the formation of a water channel pore ("the hourglass model") (*8*). Three-dimensional analysis by electron crystallography confirmed that the AQP1 monomer consists of six membrane-spanning and tilted α-helices (*9*−*11*). The six helices surround a central structure connected to helix 2 and helix 5 or 6, suggesting that the central structure is composed of loops B and E (*9*−*11*). These results, taken together with a similar observation made in MIP monomer (*12*), support the hourglass model (*8*). In addition, a chimeric study of AQP2 suggested that loops C and D are also associated with pore formation (*13*). It should be noted, however, that this result is derived from studies dealing with loss-of-function chimeras (see below), so caution is required in their interpretation.

AQP2 is a vasopressin-regulated water channel (*14*, *15*) that is indispensable for urinary concentration. Among AQPs and MIPs, AQP2 is highly homologous (58%) to MIP (AQP0), although its water channel activity is much higher than that of MIP (*16*). This distinct functional difference despite the high degree of similarity between their amino acid sequences prompted us to determine the regions responsible for the high water permeability of AQP2 by making chimeras of AQP2 and MIP. Such an attempt was previously performed by Mulders et al. with no obvious identification of the responsible regions (*17*). A major pitfall of chimeric studies is the interpretation of the loss-of-function chimeras. When a chimera loses its original function, the replaced part could very well be critical for that function, but there are also a number of other possible explanations such as a nonspecific structural change, instability of the

[†] This work was supported by a Grant-in-Aid from the Ministry of Education, Science, and Culture, Japan, and a grant from The Salt Science Research Foundation.

* To whom correspondence and reprint requests should be addressed: Second Department of Internal Medicine, School of Medicine, Tokyo Medical and Dental University, Tokyo 113-8519, Japan. Telephone: 81-3-5803-5214. Fax: 81-3-5803-5215. E-mail: mkuwmed2@med.tmd.ac.jp.

[‡] Tokyo Medical and Dental University.

[§] RIKEN.

[1] Abbreviations: AQP, aquaporin; MIP, major intrinsic protein; PCR, polymerase chain reaction; P_f, osmotic water permeability; ANOVA, analysis of variance.

10.1021/bi9916776 CCC: $18.00
Published on Web 11/11/1999

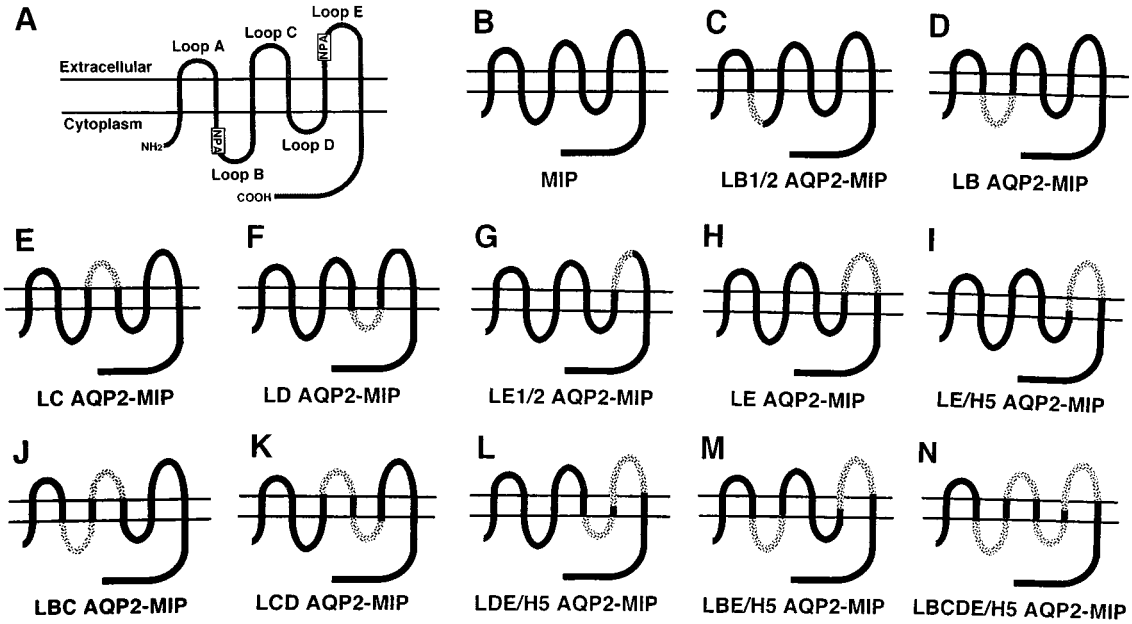

FIGURE 1: Topology of MIP and AQP and their chimeric proteins. (A) Membrane topology of MIP and AQP family members. MIP and AQP possess six presumed transmembrane helices with five connecting loops (loops A−E) and two conserved Asn-Pro-Ala (NPA) motifs in loops B and E. (B−N) MIP (B) and chimeras of AQP2 and MIP constructed in this study (C−N). Loops B−E and a part of transmembrane helix 5 of MIP were replaced by the corresponding parts of AQP2 shown with dotted lines. The chimeras were constructed with the PCR technique using wild-type MIP as a template. LX AQP2−MIP was constructed by substitution of AQP2 loop X for MIP loop X. LX1/LE2 AQP2−MIP was constructed by substitution of the front half of loop X of AQP2 for that of MIP. H5 AQP2−MIP was constructed by substitution of AQP2 helix 5 for that of MIP.

chimera RNA or protein, or a processing defect of chimera proteins between the endoplasmic reticulum and the cell surface. To account for these possibilities in the study presented here, we replaced loops B−E and transmembrane helix 5 of MIP with those of AQP2 and evaluated the results showing gain of activity, thereby allowing a more straightforward interpretation of the results.

EXPERIMENTAL PROCEDURES

Construction of the MIP and AQP2 Chimera. Chimeras of human AQP2 and bovine MIP were made with the polymerase chain reaction (PCR) technique using the MIP expression vector as a template (*18*). A fragment between *Cla*I and *Xba*I sites in pMIP/ev1 was replaced with a PCR fragment encoding the mutants. Figure 1C−N depicts the chimeras made in this study. Loops B−E (LB−LE) and a part of transmembrane helix 5 (H5) of AQP2 were substituted for those of MIP. Table 1 lists the primers used in this study. PCR was performed twice for the whole exchange of loop B, C, or E. For example, to make the LB AQP2−MIP chimera (Figure 1D), the front half of loop B was replaced using primers 1 and 2, and then the back half was replaced using primers 3 and 4. In the helix 5 chimera, a 10-residue sequence just proximal to loop E of MIP (residues 168−177, LTLGHLFGMY) was exchanged with the same sequence in AQP2 (VALGHLLGIH). To make LBC, LCD, and LDE/H5 AQP2−MIP (Figure 1J−L), PCR was carried out using a one-loop chimera as a template. To make LBE/H5 and LBCDE/H5 AQP2−MIP (Figure 1M,N), the fragment between the *Cla*I site and the *Pvu*II site (nucleotide 401) in LB and LBC AQP2−MIP (Figure 1D,J) was substituted for those of LE/H5 and LDE/H5 AQP2−MIP (Figure 1I,L), respectively. The whole DNA sequence of the constructed chimeras was confirmed by a fluorescence DNA sequencer (Applied Biosystems model 373A).

Measurement of Osmotic Water Permeability (P_f) of Oocytes. Capped RNA transcripts of wild-type AQP2, MIP, and their chimeras were synthesized in vitro with T3 RNA polymerase after a digestion with *Xba*I to linearize the plasmids. Oocytes at stage V or VI were obtained from *Xenopus laevis*. Forty nanoliters of water (Control) or 10 ng of cRNA was injected into each oocyte, and the oocytes were incubated for 48 h at 20 °C in Barth's buffer. The P_f of the oocytes was measured at 20 °C from the time course of osmotic cell swelling (*19*). The oocytes were transferred from 200 mosM Barth's buffer to 70 mosM buffer and then imaged on a CCD camera connected to an area analyzer (Hamamatsu Photonics model C3160). Serial images taken at 0.5 s intervals were stored in a computer. P_f was calculated from the initial 15 s response of cell swelling. To examine the effect of mercury on P_f, oocytes were incubated with 0.3 mM $HgCl_2$ for 5 min before the assay. To determine the reversibility of the mercurial effect, oocytes were incubated with 5 mM 2-mercaptoethanol for 15 min after the $HgCl_2$ treatment.

Preparation and P_f Measurement of Yeast Vesicles. AQP2, MIP, and their chimeras were expressed in a protease-deficient BJ3505 strain of *Saccharomyces cerevisiae* yeast cells as described previously (*20, 21*). In brief, PCR fragments of AQP2 were generated with two primers, 5′-CCCAAGCTTAGCATGTGGGAGCTCCGCTCCATA-3′ and 5′-CCCTCTAGATCAGGCCTTGGTACCCCGTGGCAG-3′ (underlining denotes *Hin*dIII and *Xba*I restriction sites, respectively), and PCR fragments of MIP and chimeras were generated with two primers, 5′-CCCAAGCTTAGCATGTGGGAACTGCGGTCAGCC-3′ and 5′-CCCTCTAGATCATCCGGGGGCTGGCTCAGCCCC-3′. These constructs were subcloned between *Hin*dIII and *Xba*I sites of a yeast expression vector, pYES2 (Invitrogen). The yeast cells were transformed with the recombinant plasmids according to a

Table 1: Oligonucleotide Primers for the Construction of AQP2−MIP Chimeras

chimera	oligonucleotide number	sequence
LB AQP2−MIP (replacement of residues 67−83)		
sense	1	5′-GGAGCCCATATCAACCCTGCAGTCACTGTCGCCTGCCTTGTGGGCTC-3′
antisense	2	5′-GAGCCCACAAGGCAGGCGACAGTGACTGCAGGGTTGATATGGGCTCC-3′
sense	3	5′-TGCCTTGTGGGCTGCCACGTGTCCGTGCTTCGTGCC-3′
antisense	4	5′-GCACGAAGCACGGACACGTGGCAGCCCACAAGGCA-3′
LC AQP2−MIP (replacement of residues 110−127)		
sense	5	5′-GTCAATGCTCTCAGCAACAGCACGACGGCTGGCCAGGCCACCATAGTGGAGATCTTC-3′
antisense	6	5′-GTCGTGCTGTTGCTGAGAGCATTGACTGCTAGGTTTCCTCGGACGGCAGGTGGGGTAAC-3′
sense	7	5′-TACAGTGTTACCCCAGCTGACATCCGAGGAGACCTAGCAGTCAATGCTCT-3′
antisense	8	5′-AGAGCATTGACTGCTAGGTCTCCTCGGATGTCAGCTGGGGTAACACTGTA-3′
LD AQP2−MIP (replacement of residues 154−157)		
sense	9	5-TACGACGAGAGGCGGGGTGAGAACCCGGGCTCCGTGGCCCTG-3′
antisense	10	5′-AGGGCCACGGAGCCCGGGTTCTCACCCCGCCTCTCGTCGTA-3′
LE AQP2−MIP (replacement of residues 181−200)		
sense	11	5′-ATGTATTATACTGGTTGCAGCATGAACCCTGCCCGCTCCCTTGCTCCTGC-3′
antisense	12	5′-AGAATGGCAGGAGCAAGGGAGCGGGCAGGGTTCATGCTGCAACCAGTATAATACAT-3′
sense	13	5′-CTTGCTCCTGCCGTTGTTACCGGAAAATTCGACGACCACTGGGTGTACTGGGT-3′
antisense	14	5′-ACCCAGTACACCCAGTGGTCGTCGAATTTTCCGGTAACAACGGCAGGAGCAAG-3′
H5 AQP2−MIP (replacement of residues 168−177)		
sense	15	5′-GCCGTTGGCTTCTCCGTCGCCCTGGGGCACCTCCTTGGGATCCATTATACTGG-3′
antisense	16	5′-CCAGTATAATGGATCCCAAGGAGGTGCCCCAGGGCGACGGAGAAGCCAACGGC-3′

lithium acetate protocol (*22*). The transformants were selected, and grown at 30 °C. The yeast vesicles were prepared as previously described (*21*, *23*). The P_f of the yeast vesicles was measured by a light-scattering method using an SX-18MV stopped-flow apparatus (Applied Photophysics Ltd.). The vesicles were diluted 1:30 with the vesicle buffer. The vesicle suspension with 300 mosM was mixed abruptly with the same volume of buffer containing 580 mM mannitol to impose a 140 mosM inwardly directed osmotic gradient. The decrease in the cell volume due to osmotic water efflux was monitored as the time-dependent increase in the 90° scattered light intensity at 466 nm. Each trace of the light intensity was obtained by averaging four to seven measurements. The light-scattering intensities were fitted to biexponential curves, and P_f was calculated as described previously (*24*, *25*) by the following equation with Mathematica software (Wolfram Research).

$$dV(t)/dt = P_f \times SAV \times vw \times [Osm_{in}/V(t) - Osm_{out}]$$

where $dV(t)$ is the volume of the cell at time *t*, SAV is the surface area-to-volume ratio at time zero (2.58×10^5 cm^{-1}, calculated from the average vesicle diameter of 233 nm measured by a Coulter counter), vw is the molecular volume of water (18 cm^3/mol), and Osm_{in} and Osm_{out} are the osmolarity inside and outside the vesicles, respectively.

Immunoblot Analysis of Oocytes and Yeast Cells. Lysates and the plasma membrane fraction of oocytes were obtained as previously described (*19*, *26*). After being heated at 70 °C for 10 min, samples were separated by SDS−PAGE. Oocyte lysates from 0.2 oocyte or plasma membrane from 20 oocytes were applied in each lane. In some experiments, oocyte lysates were incubated with endoglycosidase H (Boehringer) according to the manufacturer's instructions. The samples were transferred to Immobilon-P filters (Millipore) using a semidry system. The filters were incubated for 1 h with an affinity-purified antibody against 15 C-terminal amino acids of MIP (Sawaday Technology, Tokyo, Japan). The filters were further incubated for 1 h with a [^{125}I]-protein A solution, followed by autoradiography. For immunoblot analysis of yeast cells, vesicle fractions were isolated from MIP- or chimera-expressing yeast cells as described above. A 2.5 μg portion of protein was applied in each lane.

Immunocytochemistry of Oocytes. Oocytes were fixed in 4% paraformaldehyde for 4 h and cryoprotected overnight in phosphate-buffered saline (PBS) containing 30% sucrose. The samples were embedded in OCT compound and frozen in liquid nitrogen. Cryostat sections (6 μm) were incubated for 30 min in PBS containing 1% BSA. After three washes in PBS, the sections were incubated for 60 min with affinity-purified antibody against MIP diluted 1:500, rinsed with PBS, and further incubated for 30 min with FITC-labeled goat anti-rabbit IgG (1:200, Sigma). Oocytes were imaged with a fluorescent microscope at a magnification of 400× (Nikon BIOPHOT).

Statistics. The results were expressed as means ± the standard error. Analysis of variance (ANOVA) was used to determine statistical significance. Values for p of <0.05 were considered significant.

RESULTS

Figure 2A shows the immunoblots of the oocyte lysates. The apparent molecular mass of a 26 kDa band was detected

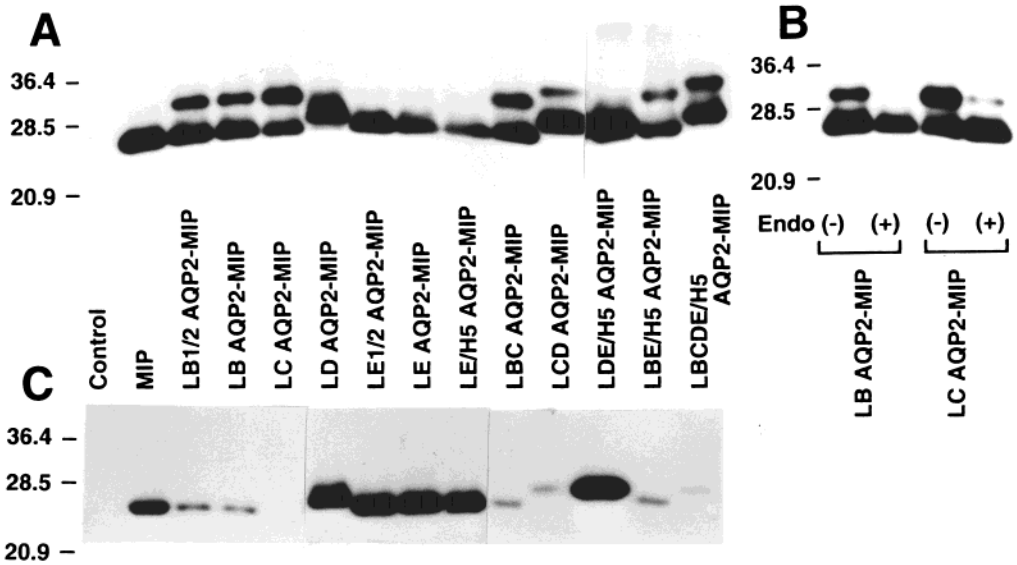

FIGURE 2: Immunoblot analysis of oocytes probed with an affinity-purified antibody against bovine MIP. Water (control) or 10 ng of cRNA of wild-type AQP2, MIP, or their chimeras was injected into oocytes. (A) Samples of the oocyte lysates. The lysates from the equivalent 0.2 oocyte were loaded in each lane. (B) Oocyte lysates before and after incubation with endoglycosidase H. (C) Samples of the plasma membrane fractions. The membranes from 20 equivalent oocytes were loaded in each lane.

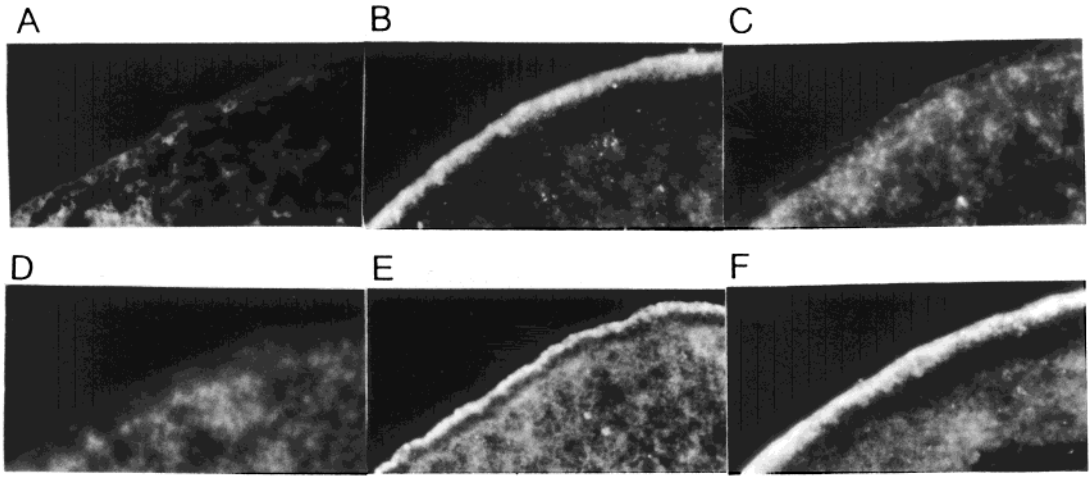

FIGURE 3: Immunocytochemistry of oocytes. Water (A) or cRNA encoding MIP (B), LB AQP2−MIP (C), LC AQP2−MIP (D), LD AQP2−MIP (E), or LE AQP2−MIP (F) was injected into oocytes. Oocyte sections were incubated with affinity-purified antibody against MIP, and immunostained with goat anti-rabbit IgG conjugated with FITC.

in oocytes to which cRNA of MIP and chimeras of loops B, C, and E had been added. In the loop D chimera, a 27 kDa band was observed. These band intensities were roughly similar in all samples. In chimeras containing the replacement of loop B or C, an additional band with a slightly higher molecular mass was identified. This extra band disappeared after digestion by endoglycosidase H (Figure 2B), indicating that it represented a glycosylated form. Because endoglycosidase H-sensitive glycoproteins are localized in endoplasmic reticulum (*27*, *28*), this observation indicated that chimeras of loops B or C might be retained in endoplasmic reticulum with an inhibition of further processing. Immunoblots of the oocyte plasma membrane fractions further disclosed the difference (Figure 2C). A clear band was detected in MIP and chimeras of loops D and E, but the band was extremely weak in chimeras having the exchange of loop B or C, indicating an impairment in the processing and cell surface appearance in these latter chimera proteins. The amount of protein expressed in the plasma membrane was estimated by densitometry. When the band density of MIP was taken to be 1, the band density was 1.21 ± 0.17, 1.15 ± 0.23, 0.94 ± 0.20, 1.08 ± 0.13, and 1.27 ± 0.18 (means $\pm$ the standard deviation, $n = 3-4$) in LD AQP2−MIP, LE1/2 AQP2−MIP, LE AQP2−MIP, LD/H5 AQP2−MIP, and LDE/H5 AQP2−MIP, respectively. These values were not significantly different from 1, suggesting that the expression levels of MIP and these chimeras in the plasma membrane were similar. Consistent with the findings in the immunoblot, the immunocytochemistry showed a bright staining of the plasma membrane in oocytes expressing loop D and loop E chimeras, whereas the plasma membrane was not stained in loop B and loop C chimeras (Figure 3).

The oocyte P_f values are summarized in Figure 4A. The P_f of water-injected oocytes (control) was $(17 \pm 2) \times 10^{-4}$ cm/s. Injection of cRNA encoding AQP2 and MIP significantly increased P_f 14.4- and 2.8-fold, respectively. AQP2 was thus 5.1 times more water permeable than MIP. P_f values were similar to the control in oocytes to which cRNA encoding LB AQP2−MIP (replacement of the whole loop B) and LC AQP2−MIP (replacement of the whole loop C)

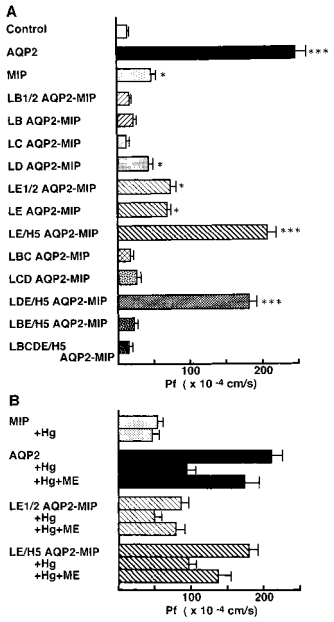

FIGURE 4: Oocyte P_f measurement. (A) Summary of P_f. Forty nanoliters of water (control) or 10 ng of cRNA encoding wild-type AQP2, MIP, or their chimeras was injected into oocytes. P_f was calculated from the time course of osmotic cell swelling of the oocytes. See Figure 1 for the structures of chimeras. Each bar represents the mean ± the standard error of 20−26 measurements. One asterisk indicates a p of <0.05 compared with the control by ANOVA; two asterisks indicate a p of <0.01 and three asterisks a p of <0.001 compared with the control by ANOVA. (B) Effect of mercury on P_f. Where indicated, the oocytes were incubated for 5 min in the presence of 0.3 mM $HgCl_2$ (+Hg) or were further incubated for 15 min in the presence of 5 mM 2-mercaptoethanol (+Hg+ME). Each bar represents the mean ± the standard error of 14−19 measurements.

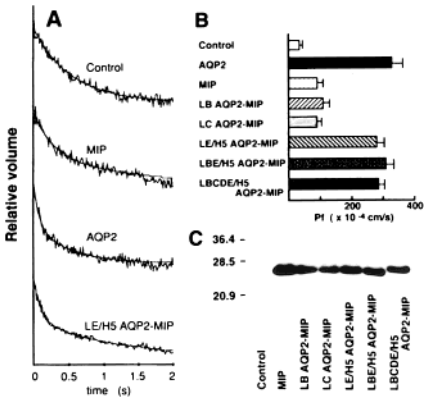

FIGURE 5: P_f measurements and immunoblot analysis of yeast cells. Wild-type AQP2, MIP, or their chimeras were expressed in yeast cells. (A) Representative traces of yeast vesicle volumes in response to osmotic shock. (B) Summary of P_f measurements. P_f was calculated from the rate of volume decrease. Each bar represents the mean ± the standard error of six to eight measurements. See Figure 1 for the structures of chimeras. (C) Immunoblots probed with affinity-purified antibody against bovine MIP. A 2.5 μg portion of protein was loaded in each lane.

had been added. These observations were consistent with the processing defects of loop B and C chimeras shown by the immunoblots (Figure 2). Injection with cRNA of LD AQP2−MIP (replacement of the whole loop D) gave a P_f similar to that of MIP, suggesting that loop D does not contribute to a high P_f. In contrast, P_f values of LE1/2 AQP2−MIP (replacement of the first half of loop E, residues 181−189) and LE AQP2−MIP (replacement of the whole loop E) were significantly higher than the P_f of MIP (p < 0.05). However, P_f values of these loop E chimeras were still 29−31% of that of AQP2, suggesting the presence of another important site for a high P_f. Because helix 5 is connected to loop E, we examined the role of this site. Surprisingly, the replacement of residues 168−177 in helix 5 together with the loop E replacement (LE/H5 AQP2−MIP) remarkably increased the P_f to (208 ± 11) × 10^{-4} cm/s. This value was not significantly different from the P_f of AQP2. Other chimeras having an exchange of loop B or C all exhibited low P_f values, primarily due to a lack of cell surface expression. LDE/H5 AQP2−MIP was appropriately expressed at the cell surface and exhibited a P_f value close to that of LE/H5 AQP2−MIP. The effects of mercury on oocyte P_f values are shown in Figure 4B. The P_f of MIP was insensitive to mercury, but the P_f of AQP2 was reversibly inhibited by mercury. A similar reversible inhibition was observed in the loop E chimera (LE1/2 AQP2−MIP) and loop E and helix 5 chimera (LE/H5 AQP2−MIP).

Because chimeras having an exchange of loop B or C failed to reach the oocyte cell surface, their role in conferring a high P_f was unknown. To examine their possible role, we used a yeast expression system, which has been shown to be free from such processing problems (*21*, *29*). The P_f of yeast vesicles was evaluated by light scattering using a stopped-flow system. Figure 5A shows representative traces. The vesicles shrunk in response to an inwardly directed osmotic gradient. The expression of MIP increased the rate of volume shrinkage, and the expression of AQP2 or LE/H5 AQP2−MIP further accelerated the rate. The rate of initial volume decrease provides a quantitative measure of P_f (Figure 5B). The P_f values of MIP- and AQP2-expressing vesicles were 2.4 and 9.0 times higher than the control P_f, respectively. The P_f of LE/H5 AQP2−MIP was comparable to that of AQP2, which confirmed the observation in oocytes (Figure 4A). Yeast P_f values of LB AQP2−MIP and LC AQP2−MIP were similar to that of MIP, clearly suggesting that chimeras containing loop B and/or C replacement did not confer a high P_f. LBE/H5 AQP2−MIP and LBCDE/H5 AQP2−MIP exhibited high P_f values equivalent to that of AQP2. Immunoblot analysis detected 26 or 27 kDa bands in all yeast cell samples (Figure 5C).

Next we replaced specific parts of helix 5 to identify the exact site responsible for a high P_f. Five amino acids differ between MIP and AQP2 in the sequence of residues 168−177 (Figure 6A). We divided this site into two parts and constructed the following four chimeras: replacement of residues168−177 (H5 AQP2−MIP), replacement of the front half of loop E (LE1/2) and residues 168−177 (LE1/2/H5 AQP2−MIP), replacement of LE1/2 and residues 174−177 (LE1/2/H5′ AQP2−MIP), and replacement of LE1/2 and residues 168 and 169 (LE1/2/H5″ AQP2−MIP). As shown in Figure 6B, a 2.7-fold increase in P_f was observed with a mere replacement of helix 5 (H5 AQP2−MIP). The P_f of LE1/2/H5 AQP2−MIP was 3.1 times higher than that of the loop E chimera (LE1/2 AQP2−MIP) and close to that of AQP2. P_f was increased 2.4-fold in LE1/2/H5′ AQP2−MIP and 2.1-fold in LE1/2/H5″ AQP2−MIP. However, these P_f values were still lower than those of LE1/2/H5 AQP2−MIP and AQP2. Finally, we constructed three chimeras of helix 5. When helix 5 of AQP2 was replaced with that of MIP

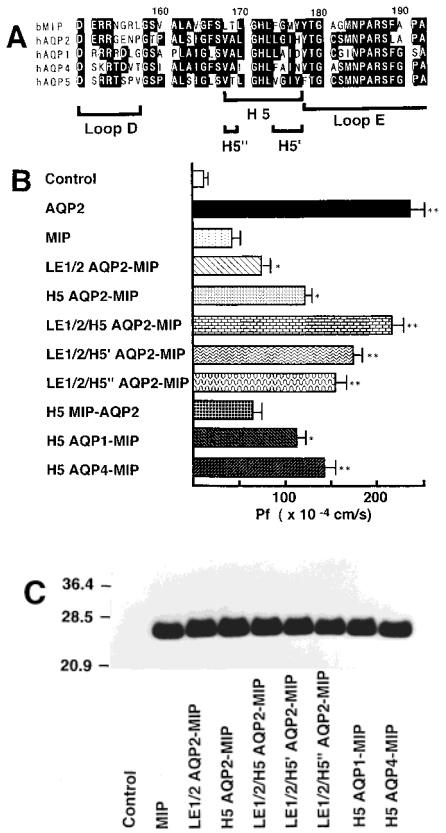

FIGURE 6: Detailed examination of transmembrane helix 5. (A) Amino acid alignment around helix 5 in MIP with AQP2, AQP1, AQP4, and AQP5. White letters in black boxes denote conserved amino acid residues. H5, H5′, and H5″ indicate residues 168−177, 174−177, and 168 and 169 in helix 5, respectively. Note that the number of amino acid residues refers to those of MIP and AQP2. (B) P_f of oocytes expressing MIP and AQP chimeras at loop E and helix 5. Forty nanoliters of water (control) or 10 ng of cRNA was injected into oocytes. Each bar represents the mean ± the standard error of 15−22 measurements. One asterisk indicates a p of <0.05 compared with that of MIP by ANOVA, and two asterisks indicate a p of <0.01 compared with that of MIP by ANOVA. (C) Immunoblots of the oocyte plasma membrane fractions probed with antibody against bovine MIP. The membranes from 20 equivalent oocytes were loaded in each lane.

(H5 MIP−AQP2), a 73% decrease in P_f was observed (Figure 6B). By contrast, P_f was increased 2.6- and 3.3-fold after helix 5 of MIP was replaced with that of AQP1 (H5 AQP1−MIP) and AQP4 (H5 AQP4−MIP), respectively. Figure 6C shows the immunoblot of plasma membrane of oocytes expressing MIP and its chimeras. The relative band densities were 1, 1.07, 0.93, 0.88, 1.14, 1.02, 1.11, and 0.95 (the mean of two separate experiments) in MIP, LE1/2 AQP2−MIP, H5 AQP2−MIP, LE1/2/H5 AQP2−MIP, LE1/2/H5′ AQP2−MIP, LE1/2/H5″ AQP2−MIP, H5 AQP1−MIP, and H5 AQP4−MIP, respectively, suggesting similar expression levels of these proteins.

DISCUSSION

Knowledge of the AQP pore structure is important for our understanding of the transport of water and small solutes through membrane proteins. One potential procedure for identifying the pore-forming regions might be a functional analysis of chimeras between a highly water-permeable AQP and an MIP family member impermeable to water. The glycerol facilitator of *Escherichia coli* is an MIP family member that permeates glycerol but not water. Thus, we initiated our experiments by replacing loop B, loop E, and several other parts of the glycerol facilitator with the corresponding parts of AQP2. However, the oocyte expression studies revealed that these chimeras were misrouted proteins whose apparent molecular masses were distinctly different from the expected sizes (M. Kuwahara, unpublished observation) and whose functions were difficult to examine. Among mammalian AQPs, MIP (AQP0), AQP1, AQP2, AQP4, and AQP5 have relatively high degrees of sequence homology and form a subgroup of AQPs. However, MIP has a much weaker water-transporting activity than the others (*16*, *30*), suggesting that it may contain the site responsible for this difference. We replaced several parts of MIP with those of AQP2 to construct gain-of-function chimeras. Some of the chimeras were correctly expressed at the plasma membrane of oocytes, but chimeras of loops B or C were not expressed at the cell surface, presumably because of misrouting (Figures 2 and 3). A similar defect in the loop B chimera was previously suggested (*17*). These misrouted chimera proteins were proved to be functional with our yeast expression system (Figure 5).

The exchange of the front half of loop E (LE1/2 AQP2−MIP) and the whole loop E (LE AQP2−MIP) significantly increased the oocyte P_f to a similar extent (Figure 4A). Thus, we can presume that the front half of loop E (residues 181−189) is involved in the stimulation of the channel function. This part contains three different residues between MIP and AQP2 (residues 181, 182, and 189, Figure 6A). C181 in AQP2 and C189 in AQP1, both located three residues proximal to the second NPA motif, are thought to be target sites for the mercurial inhibition, and the exchange of this cysteine with tryptophan was shown to decrease P_f (*13*, *31*, *32*). Thus, it was hypothesized that this cysteine participates in aqueous pore formation and that a large side chain of tryptophan causes the physical blockade of the pore (*31*, *32*). Our observation supported this view and suggested that the exchange of the front half of loop E might alter the pore structure and make it more favorable for water flow. The hourglass model of the AQP structure may predict that the role of loop B is similar to that of loop E. Our yeast vesicle studies showed that the ability to confer a high P_f is restricted to loop E and not to loop B. This observation indicates that these two loops are not completely symmetrical with regard to the function. Mulders et al. constructed the chimera of MIP with AQP2 loop E (essentially identical to LE AQP2−MIP in our study) by introducing *Age*I restriction sites at the beginning and end of this loop (*17*). In contrast to our results, the P_f of the chimera did not increase in their study. The reason for the difference between their results and ours is not clear, although residue L209 was altered to V in their chimera because of the introduction of the *Age*I site.

To our surprise, a mere replacement of 10 residues in helix 5 (residues 168−177) increased P_f 2.7-fold (Figure 6B). In addition, the P_f was comparable to that of AQP2 when we simultaneously replaced helix 5 and loop E. Conversely, P_f decreased markedly after helix 5 of MIP was spliced into AQP2. We have shown for the first time that helix 5 contributes to water permeation through AQP. Five of the residues in the exchanged part of helix 5 differ between MIP

and AQP2 (residues 168, 169, 174, 176, and 177, Figure 6A). The amino acid alignment of MIP with highly water-permeable AQPs (AQP1, -2, -4, and -5) revealed that the corresponding residues at L168 and M176 of MIP are V and I in the other four AQPs. The P_f of a partial replacement of helix 5 chimeras showed that L174−H177, and V168 and A169, are required for the maximum AQP2 activity (Figure 6B). Because helix 5 of AQP1 and AQP4 increased P_f similarly like that of AQP2 did, we speculate that the highly conserved V168 and I176 might play key roles in the expression of high water permeability in AQP1, -2, -4, and -5, and participate in the formation of the aqueous pore. It is noteworthy that these two residues are hydrophobic amino acids. A site-directed mutagenesis study of rat brain K^+ channels demonstrated that V374 has a profound effect on the ion selectivity (*33*). Then, a recent X-ray crystallography study of K^+ channels of *Streptomyces lividance* showed that the main chain atoms at positions 76−79 dominate the selectivity filter (*34*). Thus, the backbone atoms of residues 168 and 176 in helix 5 of AQPs (Figure 6A) might similarly contribute to the aqueous pathway.

It has been suggested that MIP family members are divided into two groups, namely, the water-selective channel group (e.g., MIP, AQP1, AQP2, AQP4, and AQP5) and the small molecule transporter group (e.g., glycerol facilitator, AQP3, AQP7, and AQP9) (*35*, *36*). Lagree et al. (*37*) recently showed that the serine residue at position 205 in AQPcic, an insect aquaporin, is essential for tetramerization, whereas glycerol facilitators are monomers (*37*). Thus, they suggested the possibility that water-selective channels are tetramers and small molecule transporters exist as monomers. MIP and AQP2 belong to the water-selective channel group, and the residues corresponding to S205 in AQPcic (two residues distal to the second NPA motif) are also a serine in both MIP and AQP2 (S188). Therefore, the alteration of the oligometric states might be unlikely for the functional difference among chimeras in our experiments. Lagree et al. also reported that AQPcic switched to a glycerol transporter with concomitant structural change from tetramer to monomer by the exchange of two residues (Y222 and W223) at transmembrane helix 6 (*38*). When their observations and ours are taken together, helices 5 and 6 in addition to loop E may be critical determinants for the function and structure of MIP family members.

REFERENCES

1. Preston, G. M., Smith, B. L., Zeidel, M. L., Moulds, J. J., and Agre, P. (1992) *Science 256*, 385−387.
2. Park, J. H., and Saier, M. H., Jr. (1996) *J. Membr. Biol. 153*, 171−180.
3. Haymann, J. B., Agre, P., and Engel, A. (1998) *J. Struct. Biol. 121*, 191−206.
4. Ishibashi, K., Kuwahara, M., Gu, Y., Tanaka, Y., Marumo, F., and Sasaki, S. (1998) *Biochem. Biophys. Rec. Commun. 244*, 268−274.
5. Gorin, M. B., Yancey, S. B., Cline, J., Revel, J.-P., and Horwitz, J. (1984) *Cell 39*, 49−59.
6. Preston, G. M., Jung, J. S., Guggino, W. B., and Agre, P. (1994) *J. Biol. Chem. 269*, 1668−1673.
7. Wistow, G., Pisano, M., and Chepelinsky, A. (1991) *Trends Biochem. Sci. 16*, 70−171.
8. Jung, J. S., Preston, G. M., Smith, B. L., Guggino, W. B., and Agre, P. (1994) *J. Biol. Chem. 269*, 14648−14654.
9. Walz, T., Hirai, T., Murata, K., Heymann, J. B., Mitsuoka, K., Fujiyoshi, Y., Smith, B. L., Agre, P., and Engel, A. (1997) *Nature 387*, 634−637.
10. Cheng, A., van Hoek, A. N., Yeager, M., Verkman, A. S., and Mitra, A. K. (1997) *Nature 387*, 627−630.
11. Li, H., Lee, S., and Jap, B. K. (1997) *Nat. Struct. Biol. 4*, 263−265.
12. Hasler, L., Walz, T., Tittmann, P., Gross, H., Kistler, J., and Engel, A. (1998) *J. Mol. Biol. 279*, 855−864.
13. Bai, L., Fushimi, K., Sasaki, S., and Marumo, F. (1996) *J. Biol. Chem. 271*, 5171−5176.
14. Fushimi, K., Uchida, S., Hara, Y., Hirata, Y., Marumo, F., and Sasaki, S. (1993) *Nature 361*, 549−552.
15. Sasaki, S., Fushimi, K., Saito, H., Saito, F., Uchida, S., Ishibashi, K., Kuwahara, M., Ikeuchi, T., Inui, K., Nakajima, K., Watanabe, T., and Marumo, F. (1994) *J. Clin. Invest. 93*, 1250−1256.
16. Yang, B., and Verkman, A. S. (1997) *J. Biol. Chem. 272*, 16140−16146.
17. Mulders, S. M., van der Kemp, A. J., Terlouw, S. A., van Boxtel, H. A. F., van Os, C. H., and Deen, P. M. T. (1998) *Pfluegers Arch. 436*, 599−607.
18. Kuwahara, M., Ishibashi, K., Gu, Y., Terada, Y., Kohara, Y., Marumo, F., and Sasaki, S. (1998) *Am. J. Physiol. 275*, C1459−C1464.
19. Kuwahara, M., Gu, Y., Ishibashi, K., Marumo, F., and Sasaki, S. (1997) *Biochemistry 36*, 13973−13978.
20. Kasahara, T., and Kasahara, M. (1996) *Biochem. J. 315*, 177−182.
21. Shinbo, I., Fushimi, K., Kasahara, M., Yamauchi, K., Sasaki, S., and Marumo, F. (1999) *Am. J. Physiol*. (in press).
22. Ito, H., Fuhuda, Y., Murata, K., and Kimura, A. (1983) *J. Bacteriol. 153*, 163−168.
23. Walworth, N. C., and Novick, P. J. (1987) *J. Cell Biol. 105*, 163−174.
24. Agre, P., Smith, B. L., Baumgarten, R., Preston, G. M., Pressman, E., Wilson, P., Illum, N., Anstee, D. J., Lande, M. B., and Zeidel, M. L. (1994) *J. Clin. Invest. 94*, 1050−1058.
25. Fushimi, K., Sasaki, S., and Marumo, F. (1997) *J. Biol. Chem. 272*, 14800−14804.
26. Wall, D. A., and Patel, S. (1989) *J. Membr. Biol. 107*, 189−201.
27. Halban, P. A., and Irminger, J.-C. (1994) *Biochem. J. 299*, 1−18.
28. Kuznetsov, G., and Nigam, S. K. (1998) *N. Engl. J. Med. 339*, 1688−1695.
29. Lagree, V., Pellerin, I., Hubert, J.-F., Tacnet, F., Le Caherec, F., Roudier, N., Thomas, D., Gouranton, J., and Deschamps, S. (1998) *J. Biol. Chem. 273*, 12422−12426.
30. Mulders, S. M., Preston, G. M., Deen, P. M. T., Guggino, W. B., van Os, C. H., and Agre, P. (1995) *J. Biol. Chem. 270*, 9010−9016.
31. Preston, G. M., Jung, J. S., Guggino, W. B., and Agre, P. (1993) *J. Biol. Chem. 268*, 17−20.
32. Zhang, R., van Hoek, A. N., Biwersi, J., and Verkman, A. S. (1993) *Biochemistry 32*, 2938−2941.
33. Kirsch, G. E., Drewe, J. A., Taglialatela, M., Joho, R. H., DeBiasi, M., Hartman, H. A., and Brown A. M. (1992) *Biophys. J. 62*, 136−144.
34. Doyle, D. A., Cabral, J. M., Rfuetzner, R. A., Kuo, A., Gulbis, J. M., Cohen, S. L., Chait, B. T., and MacKinnon, R. (1998) *Science 280*, 69−77.
35. Ishibashi, K., and Sasaki, S. (1998) *News Physiol. Sci. 13*, 137−142.
36. Sasaki, S., Ishibashi, K., and Marumo, F. (1998) *Annu. Rev. Physiol. 60*, 199−220.
37. Lagree, V., Froger, A., Deschamps, S., Pellerin, I., Delamarche, C., Bonnec, G., Gouranton, J., Thomas, D., and Hubert, J.-F. (1998) *J. Biol. Chem. 273*, 33949−33953.
38. Lagree, V., Froger, A., Deschamps, S., Hubert, J.-F., Delamarche, C., Bonnec, G., Thomas., D., Gouranton, J., and Pellerin, I. (1999) *J. Biol. Chem. 274*, 6817−6819.

BI9916776